INTERNATIONAL JOURNAL FOR NUMERICAL METHODS IN FLUIDS
Int. J. Numer. Meth. Fluids 2007; **55**:103–125
Published online 28 February 2007 in Wiley InterScience (www.interscience.wiley.com). DOI: 10.1002/fld.1437

Three-dimensional immersed boundary conditions for moving solids in the lattice-Boltzmann method‡

O. Erik Strack*,† and Benjamin K. Cook

Sandia National Laboratories, Albuquerque, NM 87185, U.S.A.

SUMMARY

This paper establishes the range of validity for a previously published three-dimensional moving solid boundary condition for the lattice-Boltzmann method. This method was reasonably formulated from a mass and momentum balance perspective, but was only verified for a small range of (primarily two-dimensional) problems. One of the advantages of this boundary condition is that it offers resolution at the sub-grid scale, allowing for accurate and stable calculation of the force and torque for solids which are moving through a lattice, even for small solid sizes relative to the computational grid size. We verify the boundary condition for creeping flows by comparison to analytical solutions that include both the force and the torque on fixed and moving spheres, and then follow this with comparisons to experimental and empirical results for both fixed as well moving spheres in inertial flows. Finally, we compare simulation results to numerical results of other investigators for the settling of an offset sphere and the drafting–kissing–tumbling of two sedimenting spheres. We found that an accurate calculation of the collision-operator weighting used to obtain sub-grid-scale resolution was necessary in order to prevent spikes in the velocities, forces, and moments when solid objects cross-computational cells. The wide range of comparisons collected and presented in this paper can be used to establish the validity of other numerical models, in addition to the one examined here. Published in 2007 by John Wiley & Sons, Ltd.

Received 22 December 2005; Revised 6 November 2006; Accepted 12 November 2006

KEY WORDS: computational fluid dynamics; lattice-Boltzmann; immersed boundary condition; solid–fluid interaction; particulate suspensions; domain method

*Correspondence to: O. Erik Strack, Sandia National Laboratories, Computational Shock & Multiphysics, MS 0378, P.O. Box 5800, Albuquerque, NM 87185-0378, U.S.A.
†E-mail: oestrac@sandia.gov

Contract/grant sponsor: U.S. Department of Energy; contract/grant number: DE-AC04-94AL85000
Contract/grant sponsor: ChevronTexaco
Contract/grant sponsor: Halliburton
Contract/grant sponsor: Schlumberger
Contract/grant sponsor: Shell

INTRODUCTION

Erosion, fluidization, and sedimentation are examples of problems that demand the resolution of particle–fluid interactions. In these types of problems, the mechanics of individual particles are critical to understanding the behaviour of the system as a whole. To capture the essential physics, the boundary conditions for the moving particles must be accurately resolved. Early methods pioneered by Hu *et al.* [1], Feng *et al.* [2, 3], Ladd [4, 5], Aidun and Lu [6], and Johnson and Tezduyar [7] required a large particle size relative to the computational grid or mesh spacing in order to obtain stable, consistent results, or they required re-meshing the fluid domain around the moving particles as a function of time. Recently, a large amount of research has been performed to extend both traditional computational fluid dynamics (CFD) methods and the lattice-Boltzmann method (LBM) with the objective of achieving a better representation of the surfaces of moving particles in fluids without increasing the resolution of the computational domain [8–14]. Additional work has been done in the LBM to achieve better representation of fixed boundaries that are curved [15, 16].

This paper focuses attention on a moving solid boundary condition for the LBM, presented by Noble and Torczynski [17] and later modified by Holdych [18], which resolves these issues through a modification of the lattice-Boltzmann collision operator for partially solid computational fluid cells. The Noble and Torczynski condition has not found widespread application in the literature: as of this writing, its only applications in two dimensions have been in a series of works by Cook and others [19–21], and its only application in three dimensions has been by Holdych [18]. This boundary condition was reasonably formulated from a mass and momentum balance perspective, but was only verified for a small range of problems, especially in three dimensions.

In this paper we verify Noble and Torczynski's condition for several three-dimensional problems and demonstrate its accuracy and stability for solving three-dimensional coupled particle–fluid problems. This paper will be useful to both model developers and users who wish to ascertain the range of validity of these types of coupled solid–fluid models, and to have confidence in their application to the range of problems explored in this work.

THE LATTICE-BOLTZMANN METHOD

The advantages of the LBM [22–28] over other CFD techniques is that the implementation of the method is relatively straightforward, and that complex boundaries are relatively easily implemented. In addition, the method is inherently parallel, does not require solution of a Poisson equation to recover the pressure, and does not require computation of spatial derivatives of the flow field to recover the full stress tensor (it is available in local form, see [29]). The LBM emerged from earlier work on lattice gas fluid models [27], which were based on the idea that macroscopic fluid behaviour can be modelled by the movement of packets of fluid from node to node on a regular lattice (or grid). The behaviour of these models is governed by a streaming phase, during which the packets move from node to node, and a collision phase, when the packets interact with each other. These phases are then repeated discretely through time to evolve the flow dynamics. Despite the fact that the packets move only in discrete directions and with discrete velocities, it has been shown the macroscopic, incompressible Navier–Stokes equations, with a density ρ and viscosity υ, are recovered if the fluid packets are continuous density distributions and if certain constraints are applied to the lattice and its associated collision operator [27]. The truncation error of the LBM in terms of the grid spacing, h, and time step, Δt, has been derived by Holdych *et al.* [30].

Published in 2007 by John Wiley & Sons, Ltd. *Int. J. Numer. Meth. Fluids* 2007; **55**:103–125
DOI: 10.1002/fld

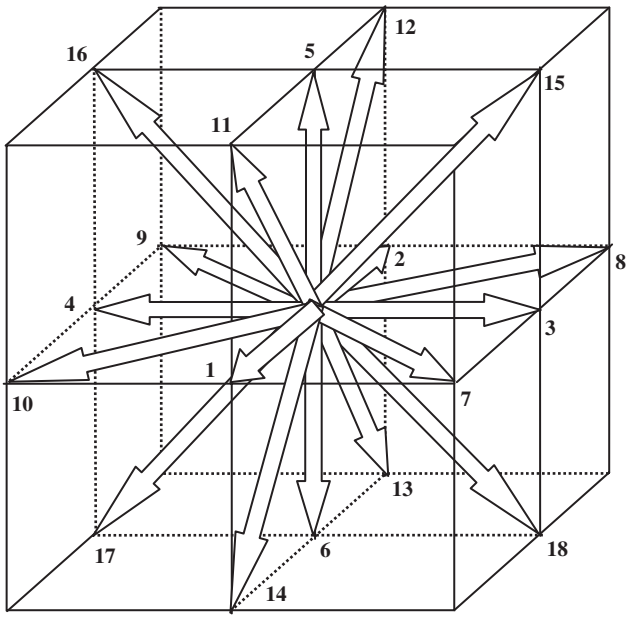

Figure 1. The D3Q19 lattice used in this study.

For our three-dimensional study we have chosen the 19-speed D3Q19 model. This choice is based on comparisons made between 15-, 19-, and 27-speed models by Mei *et al.* [31] who concluded that the 19-speed model presented the best balance between computational reliability and efficiency. The D3Q19 lattice cell used in this study is shown in Figure 1. The discrete flow velocities of the lattice are given by the vectors $\mathbf{c}_i$ where i indicates the lattice direction (in the case of the D3Q19 lattice, i runs from 0 to 18, with 0 indicating the rest, or zero, velocity). The lattice speed (the magnitude with which information propagates across the lattice) is given by $c = h/\Delta t$, where h is the spacing between lattice nodes and Δt is the time step. The magnitude of $\mathbf{c}_i$ is equal to $\sqrt{2}c$ for diagonal vectors and equal to c for all other vectors (except for $\mathbf{c}_0$, which has a magnitude of zero).

The packets of fluid are described by density distributions, which together with the lattice geometry completely describe the flow of the fluid. In this paper the distributions, given by f_i, are governed by the discrete Boltzmann equation, linearized by the BGK approximation [27, 32],

$$f_i(\mathbf{x} + \mathbf{c}_i \Delta t, t + \Delta t) = f_i(\mathbf{x}, t) - \frac{\Delta t}{\tau}(f_i(\mathbf{x}, t) - f_i^{\mathrm{eq}}(\mathbf{x}, t)) + F_i \Delta t \tag{1}$$

where the vector $\mathbf{x}$ denotes the position of the node for which the calculation is being carried out and where the relaxation parameter τ is the effective collision time between the fluid packets. The equilibrium distributions, f_i^{eq}, are specified in such a way so as to recover the Navier–Stokes equations [27]. The distributions used in our D3Q19 model [32] are given by

$$f_i^{\mathrm{eq}} = \frac{1}{3}\rho\left[1 - \frac{3}{2}\frac{\mathbf{u}^2}{c^2}\right], \quad i = 0$$

$$f_i^{\mathrm{eq}} = \frac{1}{18}\rho\left[1 + 3\frac{\mathbf{c}_i \cdot \mathbf{u}}{c^2} + \frac{9}{2}\frac{(\mathbf{c}_i \cdot \mathbf{u})^2}{c^4} - \frac{3}{2}\frac{\mathbf{u}^2}{c^2}\right], \quad i = 1\text{–}6 \tag{2}$$

$$f_i^{\mathrm{eq}} = \frac{1}{36}\rho\left[1 + 3\frac{\mathbf{c}_i \cdot \mathbf{u}}{c^2} + \frac{9}{2}\frac{(\mathbf{c}_i \cdot \mathbf{u})^2}{c^4} - \frac{3}{2}\frac{\mathbf{u}^2}{c^2}\right], \quad i = 7\text{–}18$$

where the fluid velocity at the node is given by the vector $\mathbf{u}$, which is determined by

$$\mathbf{u} = \frac{\sum_i f_i \mathbf{c}_i}{\rho} \tag{3}$$

and where the density is given by

$$\rho = \sum_i f_i \tag{4}$$

The term $F_i \Delta t$ in (1) yields a body force acting on the fluid [33]. Its magnitude is given by

$$\mathbf{G} = \sum_i F_i \mathbf{c}_i \tag{5}$$

where $\mathbf{G}$ is the imposed force. The body force term is subject to

$$\sum_i F_i = 0 \tag{6}$$

in order to conserve mass. We write [27, 34]

$$F_i = A\mathbf{G} \cdot \mathbf{c}_i \tag{7}$$

which satisfies (6). Substitution in (5) yields

$$A = \frac{1}{10c^2} \tag{8}$$

for the D3Q19 lattice used in this study. Buick and Greated [34] suggest an alternate method for incorporating a body force in the discretized Boltzmann equation (1) (comprised of an alternate computation of the velocity used in the equilibrium calculations in addition to a term similar to the one described above but with a different value for the coefficient A) that may be slightly more accurate for problems where inertial effects are dominant.

It should be noted that the LBM yields a pseudo-compressible fluid, with a benefit being that the pressure is easily computed as a function of the density using

$$p = \frac{c^2}{3}\rho \tag{9}$$

The incompressible Navier–Stokes equations are recovered with a viscosity

$$\upsilon = \frac{(2\tau^* - 1)h^2}{6\Delta t} \tag{10}$$

where the dimensionless relaxation time is given by

$$\tau^* = \frac{\tau}{\Delta t} \tag{11}$$

The accuracy of LBMs is ascertained through use of the computational Mach number

$$M = \frac{\|\mathbf{u}\|}{c} \tag{12}$$

which is proportional to the Knudson number. The 'compressibility error' [35] is on the order of M^2. Several incompressible LBMs have been proposed which remove the compressibility error at steady state, see e.g. [36, 37] and some which remove the error for general conditions e.g. [38]. In this paper we will only consider the standard LBM described above.

BOUNDARY CONDITIONS

Bounce-back boundary condition

We choose to use the bounce-back boundary method to represent no-slip conditions along stationary walls. This method simply reverses the direction of the distributions which are streamed to the bounce-back nodes. The bounce-back boundary condition has been shown to be second-order accurate in space [39] when the wall is understood to be halfway in between the bounce-back node and the fluid node. Several improved boundary conditions have been suggested in the literature [16, 40–43], however, these are more difficult to implement and also require additional computation. It should be noted that the moving boundary condition discussed in this paper can also be used to model stationary walls (by setting the velocity of the solid equal to zero).

Periodic boundary condition

Periodic boundary conditions are easily implemented in the LBM; distributions exiting the domain on one end are simply streamed (transferred) as input to the corresponding nodes at the other end.

Moving boundary condition

Attempts have been made since the early 1990s to model the coupled problem of a solid moving through a fluid. Early attempts using traditional CFD methods required re-meshing the fluid domain around the moving particles as a function of time [1, 2, 7], placing severe limitations on the ability to model large numbers of particles, especially in three dimensions. Early techniques based on the LBM [4–6, 44] required a large particle size relative to the grid spacing in order to obtain stable and consistent results. Small particle sizes relative to the grid spacing resulted in fluctuations of the forces and moments on the particles as they move across the lattice [13, 45]. Recently, several traditional and LBMs have emerged that attempt to achieve a better representation of the surfaces of moving particles in fluids without increasing the resolution of the computational domain. Glowinski *et al.* [8] adopted a fictitious domain method in the finite element method in which the forcing of the solid on the fluid is implemented through use of Lagrange multipliers. Takagi *et al.* [11] and Zhang and Prosperetti [12] proposed a new method in which part of the effect of particles moving in a fluid is represented analytically. Feng and Michaelides [13] adopted an immersed boundary method similar to the one used by Glowinski *et al.* [8] but applied it to the LBM. Verberg and Ladd's [9, 10] new lattice-Boltzmann condition attempts to resolve the boundary of a solid by bouncing back only fractions of the distributions under solid nodes.

This paper focuses attention on an immersed moving boundary condition for the LBM, presented by Noble and Torczynski [17] and later refined by Holdych [18], that modifies the collision operator

for partially solid computational fluid cells to properly impose the no-slip constraint along solid–fluid interfaces. It resolves the fluctuation of the forces and moments on the particles as they move across the lattice through a weighting of momentum exchange as a function of the fraction of the computational cell covered by the solid. We choose this approach because it allows for sub-grid-scale resolution, has proven accurate and stable in two dimensions, and has been verified for a series of two-dimensional problems including cylindrical Couette flow, sedimentation of circular and elliptical particles, and the drafting, kissing, tumbling phenomenon [19–21]. Finally, the method has also been verified for several non-trivial problems in three dimensions by Holdych [18].

Noble and Torczynski's [17] method is implemented by modifying the collision operator in the discretized Boltzmann equation for computational cells having non-zero values for the fraction of solid ε in the cell:

$$f_i(\mathbf{x}+\mathbf{c}_i\Delta t, t+\Delta t) = f_i(\mathbf{x}, t) - \frac{\Delta t}{\tau}(1-B)(f_i(\mathbf{x}, t) - f_i^{\mathrm{eq}}(\mathbf{x}, t)) + (1-B)F_i\Delta t + B\Omega_i^{\mathrm{S}} \tag{13}$$

where the parameter B is given by

$$B(\varepsilon, \tau^*) = \frac{\varepsilon(\tau^* - 1/2)}{(1-\varepsilon) + (\tau^* - 1/2)} \tag{14}$$

and where Ω_i^{S} is a new collision operator for nodes covered partially or fully by a solid. The value of the solid fraction ε varies between 0 for a completely fluid-filled cell and 1 for a completely solid cell, and as a result the value of B also varies between 0 and 1. Equation (14) returns the original collision equation for pure fluid when $B=0$, and returns the new collision operator Ω_i^{S} plus the distribution from the previous time step when $B=1$. Noble and Torczynski's [17] collision operator is given by

$$\Omega_i^{\mathrm{S}} = f_{-i}(\mathbf{x}, t) - f_{-i}^{\mathrm{eq}}(\rho, \mathbf{u}) + f_i^{\mathrm{eq}}(\rho, \mathbf{u}_{\mathrm{s}}) - f_i(\mathbf{x}, t) \tag{15}$$

where $\mathbf{u}_{\mathrm{s}}$ is the velocity of the solid, and the notation $-i$ in the distribution function subscripts indicates the distribution associated with the opposite direction of f_i. Note the straightforward implementation of the method: a single term has been added to the linearized discrete Boltzmann equation (1), and two coefficients in the equation have been modified. Only quantities already available on the mesh or easily derived (i.e. the function B and the collision operator Ω_i^{S}) are used. No additional data storage or organization is needed, which is a crucial issue in most moving boundary formulations. Calculations of the standard linearized Boltzmann equation (1) for lattice nodes that are partially or completely covered by solids are simply replaced by the modified form (13).

In order to perform a formal error analysis of this method, (15) was modified by Holdych [18]. This modified version is given by

$$\Omega_i^{\mathrm{S}} = f_{-i}(\mathbf{x}, t) - f_{-i}^{\mathrm{eq}}(\rho, \mathbf{u}_{\mathrm{s}}) + f_i^{\mathrm{eq}}(\rho, \mathbf{u}_{\mathrm{s}}) - f_i(\mathbf{x}, t) \tag{16}$$

the only difference being that the solid velocity is used to calculate the equilibrium distribution for the second term in (16).

The collision operator Ω_i^{S} given by Equations (15) and (16) is based on the concept of bounce back of the non-equilibrium part of the distributions (see [39]), which we will briefly explain here for Equation (16). When $B=1$, the last term in Equation (16) cancels the first term in Equation (13) and the entire right-hand side of Equation (13) is comprised of the first three terms

in Equation (16). The combination $f_{-i}(\mathbf{x}, t) - f_{-i}^{\mathrm{eq}}(\rho, \mathbf{u}_{\mathrm{s}})$ in (16) bounces back everything but the equilibrium distribution at the solid velocity $\mathbf{u}_{\mathrm{s}}$. The term $f_i^{\mathrm{eq}}(\rho, \mathbf{u}_{\mathrm{s}})$ is the equilibrium distribution left over from the action of the first two terms in the opposite direction.

The force and torque acting on an object covering n fluid nodes are computed by summing the new collision operator $B\Omega_i^{\mathrm{S}}$ in (13) over the nodes covered by the solid (the total momentum transferred under the solid). The force is given by

$$\mathbf{F}_{\mathrm{f}} = \frac{h^3}{\Delta t} \sum_n B_n \sum_i \Omega_i^{\mathrm{S}} \mathbf{c}_i \tag{17}$$

and the torque is given by

$$\mathbf{T}_{\mathrm{f}} = \frac{h^3}{\Delta t} \sum_n (\mathbf{x} - \mathbf{x}_{\mathrm{s}}) \times \left(B_n \sum_i \Omega_i^{\mathrm{S}} \mathbf{c}_i \right) \tag{18}$$

The second summation in both equations is over the lattice directions. The force and torque are applied to the solids in the simulations. The motion of the spheres is resolved through integration of Newton's second law, using a central finite difference scheme.

One of the strengths of the Noble and Torczynski [17] boundary condition is the way in which it treats nodes that are partially covered by solids. As solids move through the lattice, the number of computational cells that are entirely inside the solid may vary. Without a weighting for cells which are partially covered by solids, the values computed for the force and torque using (17) and (18) will jump when the number of computational cells inside the solid changes. This can lead to severely oscillating values of the force and torque acting on solids that are covered by a small number of nodes. The values oscillate less and less as more nodes cover the solid. These problems are largely eliminated by the weighting shown in (17) and (18) for computational cells that are partially covered. In simulations of a sphere moving slowly across the lattice (see the section *Force and Torque on a Settling Sphere*) we were able to recover completely smooth curves for the force and the torque as the relatively small sphere crossed the lattice. Computations involving fixed solids also benefit from a weighting of partially covered computational cells because the values of the force and torque are no longer sensitive to the position of the solid with respect to the lattice nodes. It should be noted that although this method yields smoothly varying forces and moments as solids move across the lattice, the method does not increase the resolution of the flow calculations for nodes which are not partially covered by solids. Increased resolution of the extended flow domain around the solid can only be improved by increasing the number of nodes around the solid.

NUMERICAL VERIFICATION

In this section we attempt to verify the Noble and Torczynski [17] boundary condition through comparison to several analytical solutions for creeping flows, which will demonstrate the method's ability to accurately compute the forces and torques acting on solids in a flow. In addition, we make comparisons to an empirically derived coefficient of drag in order to demonstrate its ability to capture inertial effects.

Duct flow

We demonstrate the accuracy of the base D3Q19 lattice-Boltzmann fluid solver (without boundary conditions for moving solids) by comparing our numerical results to the analytical solution for fully developed laminar flow in a square duct. Several authors have verified codes through comparison to the analytical solution for duct flow, among them Maier *et al.* [41] and Zou and He [39].

The analytical solution for the velocity u_a of a steady, incompressible flow in an infinitely long duct with a width of $2a$ in the y direction and height of $2b$ in the z direction is given by White [46]

$$u_a(y,z) = \frac{16a^2}{\rho\upsilon\pi^3}\left(-\frac{\partial p}{\partial x}\right)\sum_{k=1,3,5,\ldots}(-1)^{(k-1)/2}\left[1-\frac{\cosh(k\pi z/2a)}{\cosh(k\pi b/2a)}\right]\frac{\cos(k\pi y/2a)}{k^3} \tag{19}$$

where $-a \leqslant y \leqslant a$ and $-b \leqslant z \leqslant b$ (note that, as written, the solution is numerically unstable for large values of the term-counter k and that care must be taken to rewrite the solution for this case).

We have set up the LBM for duct flow with periodic boundaries on the upstream and downstream sides of the duct in order to simulate the infinite extent of the duct. The walls of the duct have been modelled with the bounce-back boundary condition, taking the location of the wall to be half-way between the fluid nodes closest to the wall and the bounce-back nodes. The fluid is forced into motion through use of a body force. The physical dimensions of the duct and the physical properties of the fluid are the same in all cases. The body force is held constant throughout the simulations, which effectively reduces the computational Mach number M along with the lattice spacing. The value of τ^* is also held constant throughout the simulations. Comparisons have been made for flow in a square duct because an aspect ratio of one delivers the largest errors for duct flow [41]. The results are shown in Figure 2.

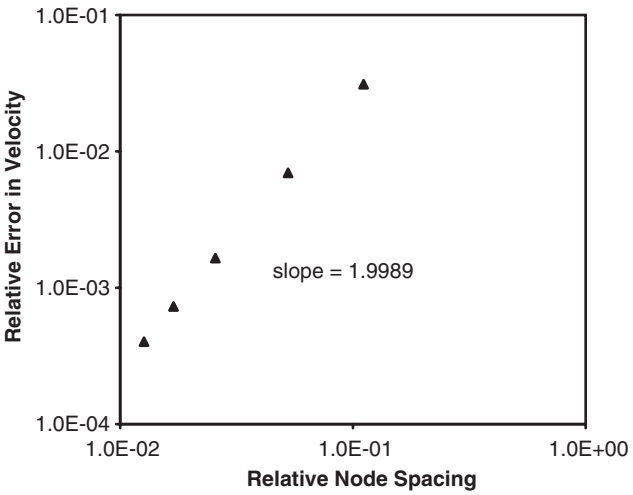

Figure 2. Relative error in velocity for flow in a square duct.

The relative error shown in Figure 2 has been computed through use of an L_2 norm calculation:

$$\text{relative error} = \sum \sqrt{\frac{(\|\mathbf{u}\| - u_a)^2}{u_a^2}} \tag{20}$$

where the summation has been taken over all the lattice nodes. The relative node spacing has been computed by dividing the node spacing h by the duct width a. As can be seen from Figure 2, near-second order accuracy has been attained. A small amount of cross-flow (flow perpendicular to the primary component of velocity in the duct) was found, which was also noted by Feng and Michaelides [47] for their lattice-Boltzmann simulations of flows in ducts containing a sphere.

Force on a sphere in Poiseuille flow

We demonstrate the accuracy of Noble and Torczynski's [17] boundary condition, as well as the accuracy of Holdych's [18] modification, for a motionless (fixed) solid by comparing numerical simulations to an approximate analytical solution for the force and torque on a fixed sphere in between two plates in a creeping Poiseuille flow. Clague and Cornelius [48] used Ladd's [4, 5] half-link boundary condition to analyse the convergence of the LBM for this particular problem. They effectively set up an infinite array of spheres in a single plane by using periodic boundary conditions on four faces of a box encompassing a sphere and bounce-back boundary conditions on the remaining two faces coinciding with the plate boundaries. As can be expected, they found the degree of convergence to the analytical solution to be a function of the effective distance separating the periodic spheres, and determined that the effect of the reflected spheres essentially vanished when the spheres were more than 30 radii apart (unfortunately, they did not quantify the remaining error). We perform the same comparison here using Noble and Torczynski's [17] boundary condition.

The approximate analytical solution [49] for the force on a sphere in creeping Poiseuille flow between two infinite, parallel walls is given by

$$F = \frac{6\pi\rho\upsilon a U[1 - (1/9)(a/l)^2]}{1 - 0.6526(a/l) + 0.3160(a/l)^3 - 0.242(a/l)^4} \tag{21}$$

where a is the sphere radius, U is the upstream fluid velocity (calculated at the periodic boundary upstream from the sphere), and l is the distance of the sphere centre to the wall. If the sphere is kept from rotating the torque is given by

$$T = \frac{8}{3}\pi\rho\upsilon a^2 U \frac{a}{l}\left[1 + 0.0758\left(\frac{a}{l}\right) + 0.049\left(\frac{a}{l}\right)^2\right] \tag{22}$$

These solutions are generated by reflecting an integral form of Stoke's solution for a single settling sphere across the wall boundaries in order to apply the no-slip condition. The solutions are approximate in nature, as only a few reflections have been calculated analytically. In our simulations we have studied the convergence of the numerical simulations for both Noble and Torczynski's [17] boundary condition as well as Holdych's [18] modification by placing a sphere between two walls $16a$ apart at a position such that $a/l = 0.25$. The lattice was $32a$ wide along the coordinate axes parallel to the walls. The walls were modelled with a bounce-back condition, and periodic conditions were used in the other two directions. The lattice spacing was refined sequentially, resulting in a reduction of the relative node spacing (the node spacing divided by the

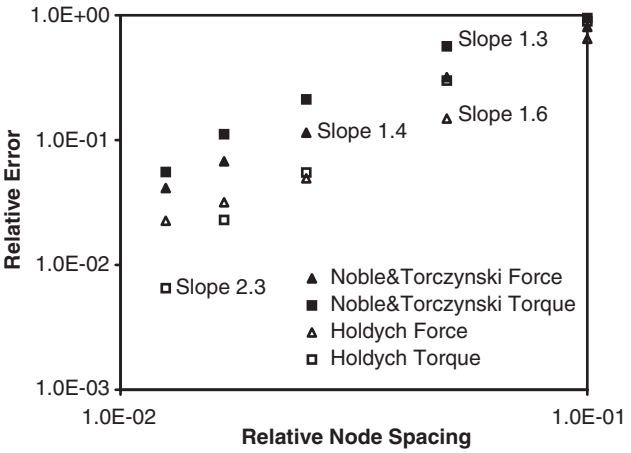

Figure 3. Comparison of relative force and torque errors for a fixed sphere in Poiseuille flow.

distance between the walls). The L_2-norm errors were computed for the simulated values, using the force and torque given by (21) and (22).

The results are shown in Figure 3, from which it is clear that both boundary conditions converge to the analytical solution. It appears that Holdych's [18] modification results in an increase in accuracy, especially for moderate values of the relative node spacing. This increase in accuracy, coupled with the fact that Holdych's [18] modification requires less computational effort (because the equilibrium distribution only needs to be computed once), is a convincing reason to consider only Holdych's [18] modification of Noble and Torczynski's [17] original method in the remainder of this paper. The slope for the torque calculated using Holdych's [18] boundary condition seems to be larger than the slope of 2.0 which is the theoretical accuracy of the LBM itself. This effect may be due to the fact that the accuracy of the torque calculation is approaching the truncation error of the analytical solution for small values of the relative node spacing.

Force and torque on a settling sphere

In the previous section we verified the boundary condition for a fixed sphere in creeping Poiseuille flow. This previous verification, however, does not test the boundary condition for cases in which a solid moves across the lattice. Aidun *et al.* [50] validated their computational method for a moving boundary condition by comparing to experimental data of Miyamura *et al.* [51] for a sphere settling in a square column of fluid. Their validation has the drawback that only values for the force on the settling sphere are given in the experimental results. We choose to verify our boundary condition for moving solids through use of a creeping flow solution for a sphere settling between two infinite plates [49], which has an expression for both the torque and the force. This analytical solution has again been obtained by using the method of reflections and is approximate in nature. The force for this solution is given by

$$F = \frac{-6\pi\rho\upsilon a U}{1 - 0.6526(a/l) + 0.1475(a/l)^3 - 0.131(a/l)^4 - 0.0644(a/l)^5} \tag{23}$$

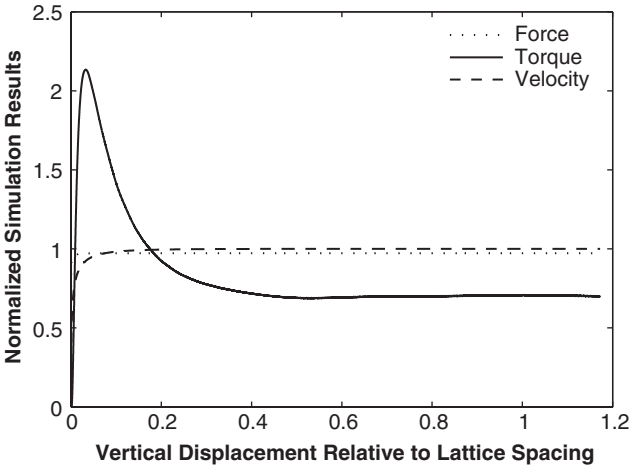

Figure 4. Normalized velocity, force, and torque values for a sphere settling between two infinite plates.

where a and l are defined as for the fixed sphere in Poiseuille flow, and where U is the velocity of the sphere. If the sphere is kept from rotating its torque is given by

$$T = \frac{0.2\pi\mu a^4 U}{l^2[1 - 0.6526(a/l)]} \tag{24}$$

which is only accurate if $(a/l)^2$ is small compared to unity. A related solution for the drag force acting on a sphere settling along the centreline between two walls and along the centreline in a circular cylinder was used by Feng and Michaelides [47] to verify their method. Feng and Michaelides [47] fixed the sphere in space and applied a velocity boundary condition along the surfaces of the infinite plates and the cylinder. In our simulation we fix the boundaries with a velocity of zero and allow the sphere to move in order to test the method for motion of the sphere across the lattice.

Our simulation was set up similarly to the simulation for a fixed sphere in Poiseuille flow described in the previous section: a sphere was placed between two walls $16a$ apart at a position such that $a/l = 0.25$. The width and depth of the lattice in the remaining two directions were set to the large value of $128a$ (as compared to the value of $32a$ used for the Poiseuille flow verifications) in order to limit sensitivity of the results to the domain size. This sensitivity is discussed in more detail later in this section. The walls were modelled with a bounce-back condition, and periodic conditions were used in the other two directions. The sphere was allowed to settle under the influence of gravity; the gravitational force on the sphere was calculated based on the density difference between the sphere and the fluid. No body force was applied to the fluid. The velocity of the sphere and the force and torque acting on the sphere are plotted in Figure 4 as a function of the vertical displacement, for a relative node spacing (node spacing divided by the plate separation) equal to 0.025. The velocity was scaled by the final settling velocity, and the force and torque were scaled by the analytical values based on the final settling velocity. The vertical displacements were scaled by the lattice spacing.

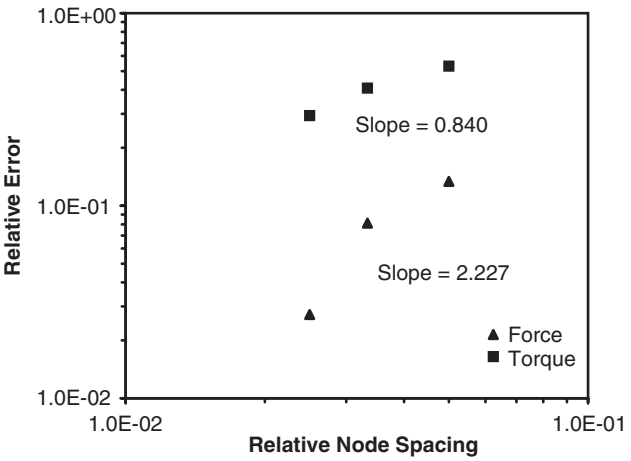

Figure 5. Relative force and torque errors for a sphere settling between two infinite plates.

A final settling velocity (in this case equivalent to a Reynolds number of 0.004) was chosen by adjusting gravity (or equivalently the density of the sphere) such that the sphere crosses at least one lattice cell. This can be seen in Figure 4 where the sphere has moved a little less than 1.2 lattice cells. The curves do not appear to be affected by traversal of computational cell boundaries. Inaccurate calculation of the solid ratio causes spikes in the velocity, force, and torque when a node that was previously covered by the solid is uncovered. Such spikes can be expected when using methods without a sub-grid-scale resolution.

An initial dynamic phase in the simulation is clearly seen in each of the curves in Figure 4. The sphere moves about two-tenths of a lattice cell before reaching a steady force and velocity. It takes much longer, approximately half a lattice cell, for the torque to reach steady state, and even then a small amount of long-wavelength oscillation can be seen during the last half of the simulation. This small amount of oscillation vanished when we ran simulations with a final Reynolds number equal to 0.00004. It is interesting to note that the torque initially overshoots the steady-state value by a substantial amount, an effect that was seen in all of our simulations (including the simulations with a very low final Reynolds number). Other than removing the small, long wavelength oscillation in the torque and velocity progressions, the results were not very sensitive to the Reynolds number, as long as the Reynolds numbers were kept small (we compared simulations with Reynolds numbers less than 0.004).

The relative errors, in an L_2 norm sense, are shown in Figure 5. The errors in each simulation were calculated by applying Equations (23) and (24) using the final settling velocity of each simulation.

In Figure 5 both the force and the torque appear to be converging as a function of the lattice spacing, but it is interesting to note that the slope of the force curve is larger than the theoretical slope of the LBM itself. This may be due to the approximate nature of the analytical solution. The small value of the slope for the torque is also of concern. This may be tied to both the approximate nature of the analytical solution for the torque (which is less accurate than the analytical solution for the force) as well as the domain size, as discussed below.

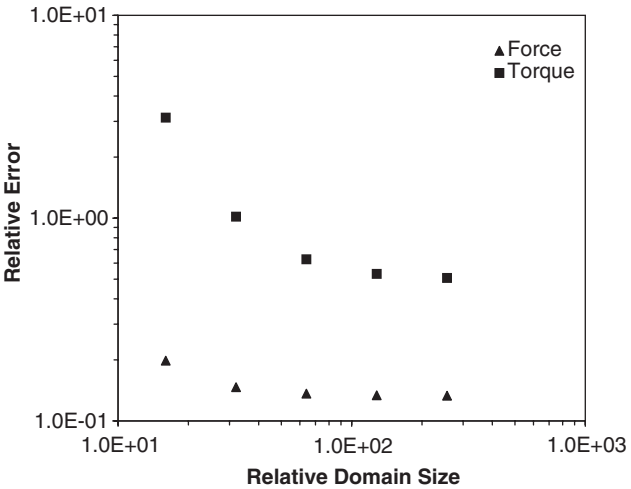

Figure 6. Relative force and torque errors as a function of relative domain size.

The simulation results for the torque were found to be very sensitive to the width and depth of the domain in the two directions parallel to the plates, as shown in Figure 6, where the relative error has been plotted *versus* the relative domain size (the length of the computational domain divided by the sphere radius), for a relative node spacing equal to 0.05.

The values for the force converge between a relative domain size of 32 and 64. The values for the torque converge much more slowly, appearing to reach a constant value between 128 and 256, perhaps even higher. This sensitivity to the domain size might be due to the small forces which generate the torque: on average the values of the torque are approximately two orders of magnitude smaller than the values of the force. The errors plotted in Figure 5 are for a relative domain size equal to 128.

Force on a settling sphere for low to moderate Reynolds numbers

In order to check Holdych's [18] boundary condition for moving boundaries in inertial flows, we allow a periodic array of spheres to settle at increasing Reynolds numbers, from Reynolds numbers of 2–40. The simulation was set up similarly to the simulation for a settling sphere between two infinite plates discussed in the previous section. A sphere was placed in a lattice box $32a$ wide in the two directions perpendicular to the direction of gravity, and $64a$ long in the direction of gravity. Periodic conditions were used on all sides of the box. A box of $80 \times 80 \times 160$ nodes was used for the results shown in Figure 7, where the numerical calculation of the drag force on the settling sphere is compared to an empirical equation for the drag coefficient given by White [46]:

$$C_{\mathrm{D}} \approx \frac{24}{Re} + \frac{6}{1+\sqrt{Re}} + 0.4 \tag{25}$$

According to White [46] this empirical formula fits the large amounts of data available within $\pm 10\%$.

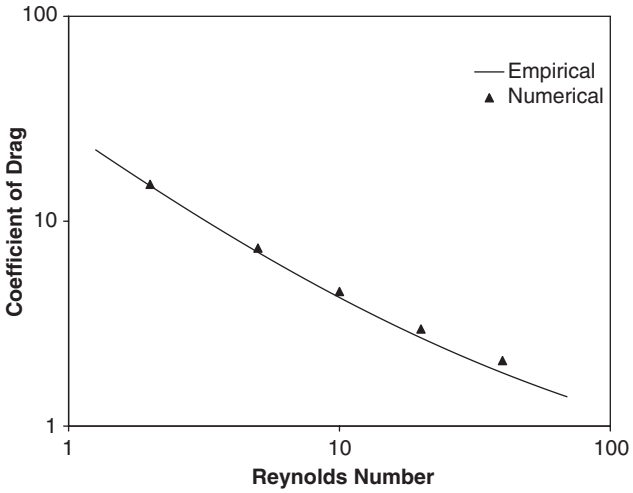

Figure 7. Drag coefficients for fixed periodic array of settling spheres.

Since we are only concerned with values for the force, the distances of separation between the periodic spheres should be sufficient for small Reynolds numbers, as seen in the convergence study for a slowly settling sphere shown in Figure 6. For larger Reynolds numbers, however, it may be expected that the effect of the spheres on each other will become increasingly apparent. This indeed appears to be the case, as can be seen in Figure 7. In these simulations the computational Mach number increases with the Reynolds number, as the simulation box was the same for all results. The final computational Mach number for a Reynolds number of 40 was 0.24, which, according to the results of Maier *et al.* [41] for duct flow with periodic boundaries, should not affect the results by more than a few percent, at most. Despite these considerations, the force on a sphere settling at a Reynolds number of 40 is within 6% of the empirical determined value.

Force on a fixed sphere for moderate Reynolds numbers

Our final comparison is one for moderate Reynolds flows, in order to test the boundary condition for flows that might realistically be found in many natural and industrial problems. Due to computer memory constraints on our serial implementation, we were not able to simulate the large domains necessary to reach Reynolds numbers on the order of 100 with settling spheres. We resorted instead to forcing fluid through a periodic array of fixed spheres. In order to reach moderate Reynolds numbers for reasonably sized lattices, we used a simulation box of $61 \times 61 \times 241$ nodes, with a relatively large sphere, which resulted in a spacing of only $6.67a \times 6.67a \times 26.7a$. With this coarse configuration, we are merely attempting to demonstrate that the method can achieve Reynolds numbers on the order of 100 while still matching observed behaviour in a rough sense. The results for the force calculated numerically are again compared to the empirical formula for the coefficient of drag given in Equation (25), as well as to some experimental results published by Roos and Willmarth [52], shown in Figure 8. The results appear to be within $\pm 10\%$ of the empirical curve, despite the relatively crude nature of the comparison.

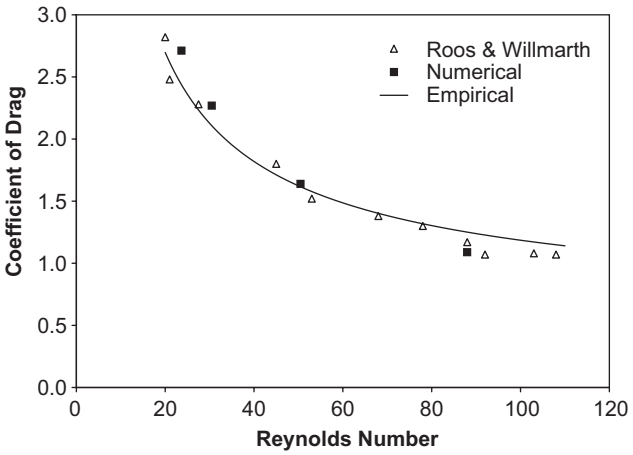

Figure 8. Drag coefficients for flow through a fixed periodic array of spheres.

SIMULATION RESULTS FOR A SETTLING SPHERE

After having verified the model for both moving and fixed boundaries we will now demonstrate its ability to model the dynamic phenomena of settling spheres.

Single settling sphere in a column of fluid

If a single, offset sphere is dropped in a column of fluid, it will oscillate around the centreline of the column for certain Reynolds numbers and certain column widths, as discussed by Feng and Michaelides [47] for spheres and by Feng *et al.* [2] for two-dimensional disks and cylinders, and previously simulated in two dimensions using Noble and Torczynski's condition [19, 20].

This oscillating behaviour is caused by the lift force generated by the presence of a wall near a settling particle in inertial flows and is absent in non-inertial flows (such as in the verification discussed in the previous section [49]).

In order to simulate this behaviour we set up several simulations similar to the ones that were run by Feng and Michaelides [47]. A sphere with a diameter of D is placed in a square channel $L \times L$ wide and $16L$ deep, at a location $0.4L$ from one of the sides. The ratio of D/L is approximately equal to $\frac{2}{3}$. The sphere is allowed to settle under the influence of gravity, and the magnitude of gravity (or, equivalently the density of the sphere) is adjusted in order to change the magnitude of the settling velocity. The coordinate axes are aligned parallel to the boundaries of the column, with the y-axis pointing in the direction of gravity along the depth of the column. Periodic conditions are used at the intersection of the y-axis and at the two ends of the column. Bounce-back conditions are used along the remaining four sides of the column. The results of the simulations are shown in Figure 9.

The results in Figure 9 qualitatively agree with those presented by Feng and Michaelides [47]. Even though the Reynolds numbers (defined by the terminal velocity and diameter of the sphere) do not match exactly, it is apparent that the peak values of the oscillations, as well as the intersections with the centreline, have nearly the same values for the first three cycles. It appears, however, that

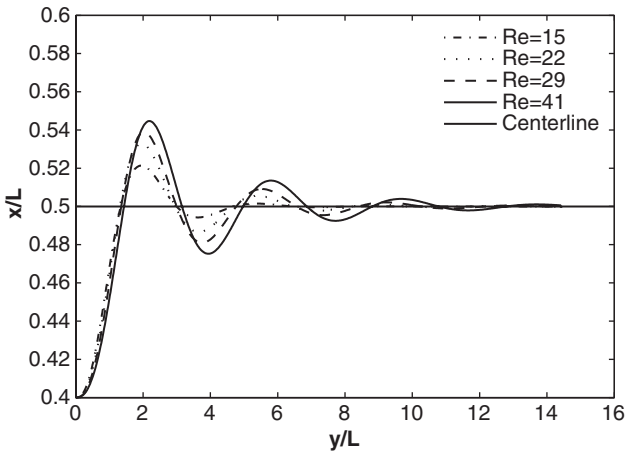

Figure 9. Oscillation curves for a single sphere settling in a square column of fluid.

the oscillations damp out more quickly in our results than those presented in Feng and Michaelides [47]. This is especially noticeable after the sphere has passed the centreline for the fourth time. This difference may be due to the different methods used to apply the boundary conditions on the surface of the sphere, which could cause different forces to be applied to the settling spheres. Another possibility is the differing boundary conditions applied at the top and bottom of the column of fluid. We apply periodic boundary conditions, whereas Feng and Michaelides [47] apply a zero stress ($\mathrm{d}v_y/\mathrm{d}y = 0$) condition.

Drafting–kissing–tumbling

The phenomenon of two particles drafting, kissing, and tumbling in a column of fluid was first reported by Joseph *et al.* [53], and the results of two-dimensional simulations using both traditional and LBMs were given by Hu *et al.* [1], Feng *et al.* [2], Glowinski *et al.* [8], Qi [44], and Patankar *et al.* [54]. The phenomenon has also been captured in two-dimensional simulations using the Noble and Torczynski's condition [19, 20]. Three-dimensional simulations were reported by Qi [44] and Glowinski *et al.* [8]. We attempt to duplicate the three-dimensional results published by Qi [44]. Our model does not include corrections for lubrication forces which are generated when two solids in a fluid are near contact. Such forces can be important in these types of simulations, and may be included in a relatively straightforward manner, see, for example, Ding and Aidun [55] and Nguyen and Ladd [56].

The drafting–kissing–tumbling simulation was set up similarly to the one described above for a single settling sphere. The details are as follows. Two offset spheres each with a diameter of D are placed in a square channel $L \times L$ wide and $16L$ deep, with a ratio of D/L equal to 0.2. The coordinate axes are aligned parallel to the boundaries of the column, with the y-axis pointing in the direction of gravity along the depth of the column and the origin placed in the upper-left corner of the front face. Periodic conditions are used at the intersection of the y-axis and the two ends of the column. Bounce-back conditions are used along the remaining four sides of the column. The first sphere is placed at the (x, y, z) coordinates of $(2.032D, 3.96D, 2.5D)$, and the second

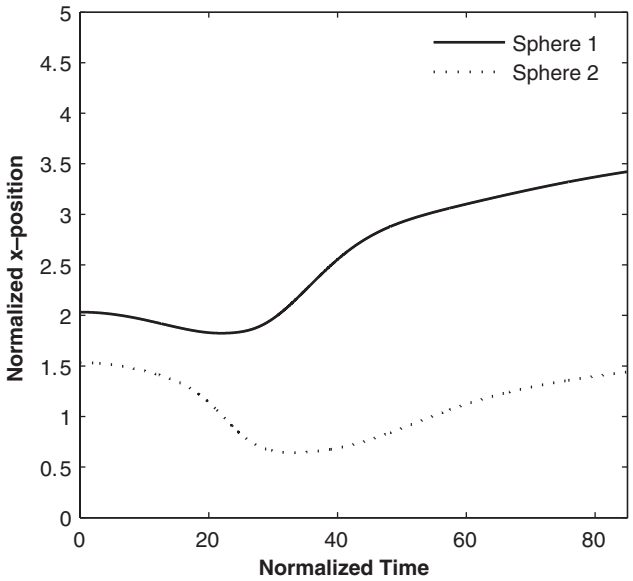

Figure 10. Sphere positions in the x-direction as a function of time.

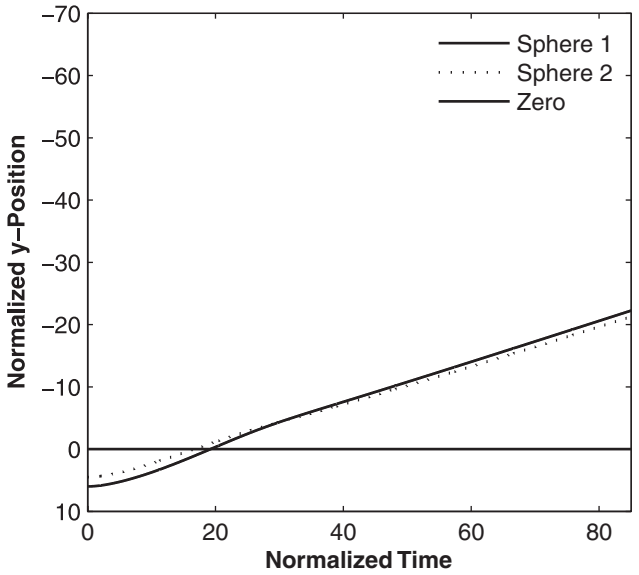

Figure 11. Sphere positions in the y-direction as a function of time.

sphere is placed at the coordinates $(1.532D, 5.46D, 2.5D)$. The spheres have a density equal to 1.005 times the density of the fluid and are allowed to settle under the influence of gravity. The results of the simulations are shown in Figures 10–15.

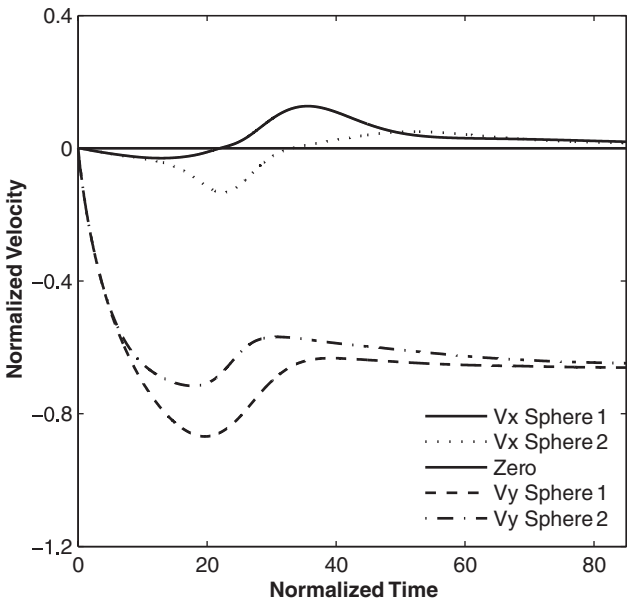

Figure 12. Sphere velocities in the *x*- and *y*-direction as a function of time.

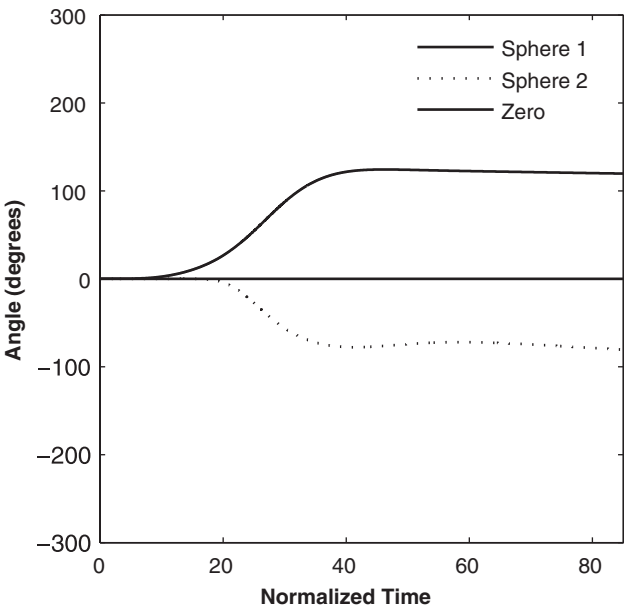

Figure 13. Sphere rotations as a function of time.

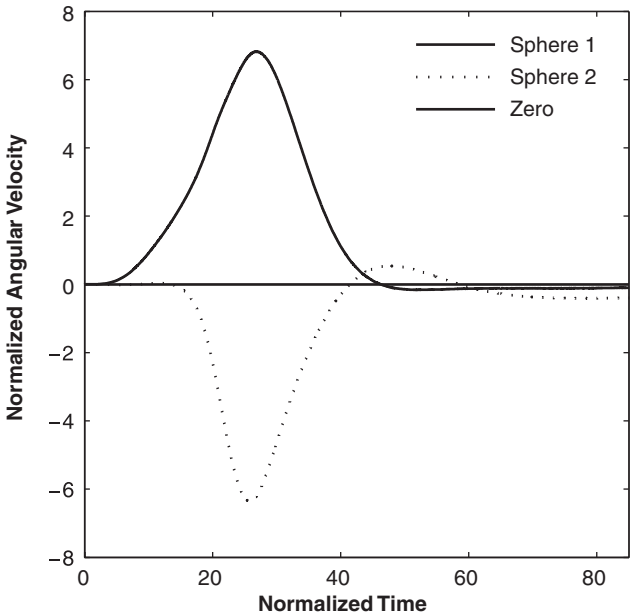

Figure 14. Sphere angular velocities as a function of time.

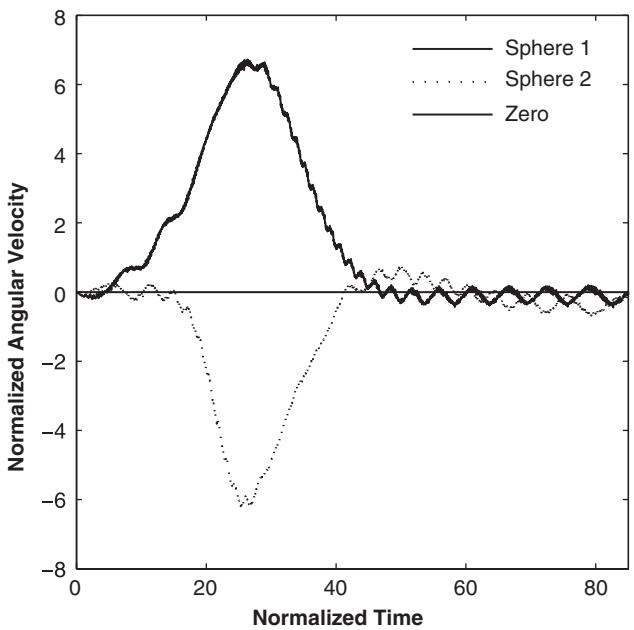

Figure 15. Sphere angular velocities as a function of time, calculated without sub-grid-scale resolution.

The variables shown in the plots have been normalized as follows. The positions have been scaled by D. The velocities have been scaled by the final velocity as calculated by Qi [44]: $U_f = \upsilon Re_f / r$ where r is the radius of each of the spheres, and where Re_f is the average final Reynolds number of the two spheres at the end of Qi's [44] simulation, given in his paper as 13.1. Time and angular velocity have been scaled by the quantity r/U_f.

We have used periodic conditions on the two ends of the column in the y-direction whereas Qi [44] applied a stress-free boundary condition, setting the derivatives of the flow velocity equal to zero in the x- and y-directions. In addition, Qi [44] moved his boundary along with the particles, keeping the boundary $15D$ ahead and $20D$ behind the spheres. We have kept our boundaries fixed in a domain $20D$ deep. The different boundary conditions appear to have a strong influence on the results of the simulation, especially after the first sphere catches the second sphere, around $tU_f/r = 30$. Especially noticeable is that the spheres in Qi's [44] simulation continue to accelerate after the spheres pass one another, whereas the spheres in our simulation reach a terminal velocity. By changing the gravity (or, equivalently, the density of the particles or the viscosity) we varied the final Reynolds numbers in the simulation. In every case (with the same initial geometry) both particles reached terminal velocity by the end of the simulation. This has been corroborated by Qi (private communication, 2004), who kindly performed a low-resolution version of the same simulation with zero-velocity boundary conditions at the top and bottom of the column. In this case, his spheres also reached a terminal velocity, close to our terminal velocity.

Despite the discrepancies for later times, the overall behaviour of the simulations is qualitatively similar. Both the positions and velocities in the x-direction are very close, especially for the first 50 time units or so. As mentioned above, the vertical velocities are quite different, even before the first sphere passes the second sphere, in that the velocities level out somewhat before they pass each other. The most likely cause for this difference is in the implementation of the no-slip boundary conditions for the moving spheres. Ladd's [4, 5] boundary condition, which is used in Qi's [44] implementation, does not have a mechanism for dealing with partially solid computational cells (sub-grid resolution), which is likely to have the most effect when the spheres are close.

The rotation of the spheres is very similar up to about 30 time units into the simulation, when the spheres in Qi's [44] simulation continue to rotate, whereas the spheres in Figure 13 stop rotating almost completely. This can also be seen by comparing the angular velocities. The angular velocities in Qi's [44] simulation reach a relatively constant value after approximately 35 time units, whereas the velocities in Figure 14 are nearly exactly zero after about 40 time units. Another noticeable difference in the angular velocities is the ragged nature of Qi's [44] values versus the much smoother values in Figure 14. The most likely cause for the raggedness in Qi's [44] results for the angular velocity is the fact that his computations do not have a sub-grid-scale resolution. This likely cause is illustrated in Figure 15, where we have performed our computations without any sub-grid-scale resolution (i.e. the parameter B in Equation (14) is only allowed to assume values of one or zero), resulting in similar undulations in the velocity values.

CONCLUSION

This paper presents several three-dimensional verifications of a moving solid boundary condition for the LBM that was originally developed by Noble and Torczynski [17] and later verified in two dimensions by Cook [19–21]. We also examined a modification of the method suggested by Holdych [18], which we found to be more computationally efficient and more accurate in the

verifications performed for this paper. The boundary conditions studied in this paper have the advantage that accurate and stable values for the force and torque are obtained for solids which are moving through a lattice, even for small particle sizes relative to the computational grid size.

We verified the boundary condition for creeping flows by comparison to analytical solutions that include both the force and the torque on fixed and moving spheres, and then followed this with comparisons to experimental and empirical results for both fixed as well moving spheres in inertial flows. Finally, we compared our simulation results to numerical results of other investigators for more complicated behaviours, such as the settling of an offset sphere and the drafting–kissing–tumbling of two sedimenting spheres. We emphasized the importance of the weighting of the fluid forcing for computational cells that are only partially covered by a solid. Without an accurate calculation of this weighting we found that our results showed spikes in the velocities, forces, and moments when crossing computational cells. The wide range of comparisons presented clearly establishes the range of validity for this boundary condition, and can also be used to verify other boundary conditions and numerical codes.

ACKNOWLEDGEMENTS

The authors are grateful to Professor Dewei Qi who kindly ran several drafting–kissing–tumbling simulations at our request. The authors would also like to thank David Boutt for many valuable conversations and David Noble and David Holdych for both their insights and their efforts in reviewing this paper. Finally, we are grateful to an anonymous reviewer who suggested several improvements to the paper. Funding for this research was provided by the U.S. Department of Energy through the Natural Gas and Oil Technology Partnership, and a cooperative research and development agreement with ChevronTexaco, Halliburton, Schlumberger, and Shell. Sandia is a multiprogram laboratory operated by the Sandia Corporation, a Lockheed Martin Company, for the United States Department of Energy's National Nuclear Security Administration under Contract DE-AC04-94AL85000.

REFERENCES

1. Hu HH, Joseph DD, Crochet MJ. Direct simulation of fluid particle motions. *Theoretical and Computational Fluid Dynamics* 1992; **3**:285–306.
2. Feng J, Hu HH, Joseph DD. Direct simulation of initial-value problems for the motion of solid bodies in a Newtonian fluid. Part 1. Sedimentation. *Journal of Fluid Mechanics* 1994; **261**:95–134.
3. Feng J, Hu HH, Joseph DD. Direct simulation of initial-value problems for the motion of solid bodies in a Newtonian fluid. Part 2. Couette and Poiseuille flows. *Journal of Fluid Mechanics* 1994; **277**:271–301.
4. Ladd AJC. Numerical simulations of particulate suspensions via a discretized Boltzmann equation. Part 1. Theoretical foundation. *Journal of Fluid Mechanics* 1994; **271**:286–309.
5. Ladd AJC. Numerical simulations of particulate suspensions via a discretized Boltzmann equation. Part 2. Numerical results. *Journal of Fluid Mechanics* 1994; **271**:311–339.
6. Aidun CK, Lu Y. Lattice Boltzmann simulation of solid particles suspended in fluid. *Journal of Statistical Physics* 1995; **81**(1–2):49–61.
7. Johnson AA, Tezduyar T. Simulation of multiple spheres falling in a liquid-filled tube. *Computer Methods in Applied Mechanics and Engineering* 1996; **134**:351–373.
8. Glowinski R, Pan T-W, Hesla TI, Joseph DD. A distributed Lagrange multiplier/fictitious domain method for particulate flows. *International Journal of Multiphase Flow* 1999; **25**:755–794.
9. Verberg R, Ladd AJC. Lattice-Boltzmann model with sub-grid-scale boundary conditions. *Physical Review Letters* 2000; **84**(10):2148–2151.
10. Verberg R, Ladd AJC. Accuracy and stability of a lattice-Boltzmann model with subgrid scale boundary conditions. *Physical Review E* 2001; **65**(016701):1–16.
11. Takagi S, Oğuz HN, Zhang Z, Prosperetti A. PHYSALIS: a new method for particle simulation. Part II: Two-dimensional Navier–Stokes flow around cylinders. *Journal of Computational Physics* 2003; **187**:371–390.

12. Zhang Z, Prosperetti A. A method for particle simulation. *Journal of Applied Mechanics* 2003; **70**:64–74.
13. Feng Z-G, Michaelides EE. The immersed boundary-lattice Boltzmann method for solving fluid–particles interaction problems. *Journal of Computational Physics* 2004; **195**:602–628.
14. Li H, Fang H, Lin Z, Xu S-X, Chen S. Lattice Boltzmann simulation on particle suspensions in a two-dimensional symmetric stenotic artery. *Physical Review E* 2004; **69**:031919-1-9.
15. Filippova O, Hänel D. Lattice-Boltzmann simulation of gas-particle flow in filters. *Computers and Fluids* 1997; **26**(7):697–712.
16. Mei R, Luo L-S, Shyy W. An accurate curved boundary treatment in the lattice Boltzmann method. *Journal of Computational Physics* 1999; **155**:307–330.
17. Noble DR, Torczynski JR. A lattice Boltzmann method for partially saturated computational cells. *International Journal of Modern Physics C* 1998; **9**(9):1189–1201.
18. Holdych DJ. Lattice Boltzmann methods for diffuse and mobile interfaces. *Ph.D. Thesis*, University of Illinois at Urbana, Champaign, 2003.
19. Cook BK, Noble DR, Preece DS, Williams JR. Direct simulations of particle-laden fluids. In *Pacific Rocks 2000*, Girard, Liebman, Breeds, Doe (eds). Balkema: Rotterdam, 2000; 279–286.
20. Cook BK. A numerical framework for the direct simulation of solid–fluid systems. *Ph.D. Thesis*, Massachusetts Institute of Technology, 2001.
21. Cook BK, Noble DR, Williams JR. A direct simulation method for particle–fluid systems. *Engineering Computations* 2004; **21**(2):151–168.
22. Higuera FJ, Succi S, Benzi R. Lattice gas-dynamics with enhanced collisions. *Europhysics Letters* 1989; **9**(4): 345–349.
23. Higuera FJ, Jimenez J. Boltzmann approach to lattice gas simulations. *Europhysics Letters* 1989; **9**:663–668.
24. Chen H, Chen S, Matthaeus WH. Recovery of the Navier–Stokes equations using a lattice-gas Boltzmann method. *Physical Review A* 1992; **45**:R5339–R5342.
25. Benzi R, Succi S, Vergassola M. The lattice Boltzmann equation: theory and applications. *Physics Reports* 1992; **222**(3):145–197.
26. Chen S, Doolen GD. Lattice Boltzmann method for fluid flows. *Annual Review of Fluid Mechanics* 1998; **30**:329–364.
27. Wolf-Gladrow DA. *Lattice-Gas Cellular Automata and Lattice Boltzmann Models*. Springer: Berlin, 2000.
28. Succi S. *The Lattice Boltzmann Equation for Fluid Dynamics and Beyond*. Oxford University Press: Oxford, 2001.
29. Rossi N, Ubertini S, Bella G, Succi S. Unstructured lattice Boltzmann method in three dimensions. *International Journal for Numerical Methods in Fluids* 2005; **49**(6):619–633.
30. Holdych DJ, Noble DR, Georgiadis JG, Buckius RO. Truncation error analysis of lattice Boltzmann methods. *Journal of Computational Physics* 2004; **193**:595–619.
31. Mei R, Shyy W, Yu D, Lou L-S. Lattice Boltzmann method for 3-D flows with curved boundary. *Journal of Computational Physics* 2000; **161**:680–699.
32. Koelman JMVA. A simple lattice Boltzmann scheme for Navier–Stokes fluid flow. *Europhysics Letters* 1991; **15**(6):603–607.
33. Noble DR, Georgiadis JG, Buckius RO. Comparison of accuracy and performance for lattice Boltzmann and finite difference simulations of steady viscous flow. *International Journal for Numerical Methods in Fluids* 1996; **23**:1–18.
34. Buick JM, Greated CA. Gravity in a lattice Boltzmann model. *Physical Review E* 2000; **61**(5):5307–5320.
35. Reider M, Sterling J. Accuracy of discrete-velocity BGK models for the simulation of the incompressible Navier–Stokes equations. *Computers and Fluids* 1995; **24**(4):459–467.
36. Zou QS, Hou SL, Chen SY, Doolen GD. An improved incompressible lattice Boltzmann model for time-independent flows. *Journal of Statistical Physics* 1995; **81**(1–2):35–48.
37. He X, Luo L-S. Lattice Boltzmann model for the incompressible Navier–Stokes equation. *Journal of Statistical Physics* 1997; **88**(3–4):927–944.
38. Guo Z, Shi B, Wang N. Lattice BGK model for incompressible Navier–Stokes equation. *Journal of Computational Physics* 2000; **165**:228–306.
39. Zou QS, He XY. On pressure and velocity boundary conditions for the lattice Boltzmann BGK model. *Physics of Fluids* 1997; **9**(6):1591–1598.
40. Noble DR, Chen SY, Georgiadis JG, Buckius RO. A consistent hydrodynamic boundary condition for the lattice Boltzmann method. *Physics of Fluids* 1995; **7**(1):203–209.

Published in 2007 by John Wiley & Sons, Ltd. *Int. J. Numer. Meth. Fluids* 2007; **55**:103–125
DOI: 10.1002/fld

41. Maier RS, Bernard RS, Grunau DW. Boundary conditions for the lattice Boltzmann method. *Physics of Fluids* 1996; **8**(7):1788–1801.
42. Ansumali S, Karlin IV. Kinetic boundary conditions in the lattice Boltzmann method. *Physical Review E* 2002; **66**(2):026311/1-6.
43. Sbragaglia M, Succi S. Analytical calculation of slip flow in lattice Boltzmann models with kinetic boundary conditions. *Physics of Fluids* 2005; **17**(9):93602/1-8.
44. Qi D. Lattice-Boltzmann simulations of particles in non-zero-Reynolds-number flows. *Journal of Fluid Mechanics* 1999; **385**:41–62.
45. Ladd AJC. Sedimentation of homogeneous suspensions of non-Brownian spheres. *Physics of Fluids* 1997; **9**(3):491–499.
46. White FM. *Viscous Fluid Flow* (2nd edn). McGraw-Hill: New York, 1991.
47. Feng Z-G, Michaelides EE. Hydrodynamic force on spheres in cylindrical and prismatic enclosures. *International Journal of Multiphase Flow* 2002; **28**:479–496.
48. Clague DS, Cornelius PJ. The hydrodynamic force and torque on a bounded sphere in Poiseuille flow. *International Journal for Numerical Methods in Fluids* 2001; **35**:55–70.
49. Happel J, Brenner H. *Low Reynolds Number Hydrodynamics with Special Applications to Particulate Media* (revised 2nd edn). Martinus Nijhoff Publishers: The Hague, 1983.
50. Aidun CK, Lu Y, Ding E-J. Direct analysis of particulate suspensions with inertia using the discrete Boltzmann equation. *Journal of Fluid Mechanics* 1998; **373**:287–311.
51. Miyamura A, Iwasaki S, Ishii T. Experimental wall correction factors of single solid spheres in triangular and square cylinders, and parallel plates. *International Journal of Multiphase Flow* 1981; **7**(1):41–46.
52. Roos FW, Willmarth WW. Some experimental results on sphere and disk drag. *AIAA Journal* 1971; **9**:285–291.
53. Joseph DD, Fortes AF, Lundgren TS, Singh P. Nonlinear mechanics of fluidization of beds of spheres, cylinders and disks in water. In *Advances in Multiphase Flow and Related Problems*, Papanicolau G (ed.). SIAM: Philadelphia, PA, 1987; 101–122.
54. Patankar NA, Singh P, Joseph DD, Glowinski R, Pan T-W. A new formulation of the distributed Lagrange multiplier/fictitious domain method for particulate flows. *International Journal of Multiphase Flow* 2000; **26**: 1509–1524.
55. Ding E-J, Aidun CK. Extension of the lattice-Boltzmann method for direct simulation of suspended particles near contact. *Journal of Statistical Physics* 2003; **112**(3/4):685–708.
56. Nguyen N-Q, Ladd AJC. Lubrication corrections for lattice-Boltzmann simulations of particle suspensions. *Physical Review E* 2002; **66**:046708-1-12.